

Strain-controlled nanocrack formation in a Pd film on polydimethylsiloxane for the detection of low H₂ concentrations

**Sungyeon Kim, Hyun-Sook Lee,
Byungjin Jang, Sungmee Cho &
Wooyoung Lee**

Journal of Materials Science

Full Set - Includes 'Journal of Materials
Science Letters'

ISSN 0022-2461

J Mater Sci

DOI 10.1007/s10853-016-9765-2



Your article is protected by copyright and all rights are held exclusively by Springer Science +Business Media New York. This e-offprint is for personal use only and shall not be self-archived in electronic repositories. If you wish to self-archive your article, please use the accepted manuscript version for posting on your own website. You may further deposit the accepted manuscript version in any repository, provided it is only made publicly available 12 months after official publication or later and provided acknowledgement is given to the original source of publication and a link is inserted to the published article on Springer's website. The link must be accompanied by the following text: "The final publication is available at link.springer.com".

Strain-controlled nanocrack formation in a Pd film on polydimethylsiloxane for the detection of low H₂ concentrations

Sungyeon Kim¹ · Hyun-Sook Lee¹ · Byungjin Jang¹ · Sungmee Cho¹ · Wooyoung Lee¹

Received: 22 October 2015 / Accepted: 19 January 2016
© Springer Science+Business Media New York 2016

Abstract We report quantitative nanocrack formation upon adjusting the mechanical tensile strain applied to a Pd thin film on an elastomeric polydimethylsiloxane (PDMS) substrate and its detection properties for H₂ gas in air. Nanocrack formation in Pd/PDMS substrates was controlled through the application of tensile strains that varied in the range 30–120 % during mechanical stretching/compression. This method can be used to modulate nanocrack formation along both the *x*- and *y*-axes over a large area. Increasing the applied tensile strain to 90 % induced the appearance of horizontal cracks along the *y*-axis in addition to an increased number of vertical cracks along the *x*-axis. When the strain reached 120 %, ordered nanocracks abundantly propagated on the Pd surface in both the directions. Gas detection properties were dramatically enhanced, with a very low detection limit of 50 ppm H₂ in air observed for 120 % strain. This was attributed to the large surface area in the Pd nanocrack pattern, which readily allowed for volume expansion. These results provide a simple mechanism for

controlling the detection properties of H₂ gas sensors with low detection limits in air.

Introduction

Hydrogen is a promising resource for many applications, especially for hydrogen vehicles and in the semiconductor industry; it also has the potential for development as an energy carrier. However, owing to the flammability and explosive nature of hydrogen, secure monitoring systems and H₂ gas sensors are needed. Many efforts have focused on developing H₂ gas sensors with rapid response times and high sensitivities and selectivities. To develop a sensor that operates with a low detection threshold at ambient temperature, H₂ gas sensors have been fabricated using Pd metal films due to their superior hydrogen solubility properties at ambient temperature, compared to metal-oxide-based sensors (ZnO, WO₃, In₂O₃, NiO, CuO, Fe₂O₃, TiO₂, MnO₃, and SnO₂), which typically operate at relatively high temperatures (~400 °C) [1–9].

We have previously reported examples of controlled nanogap formation for H₂ sensors by either the stretching or repeated H₂ treatment cycles of Pd films on elastomeric substrates, which showed satisfactory ON–OFF behaviors and rapid response times (<1 s) [10–16]. Through these studies, we showed that the reduction of the nanogap width is a key to achieving a low detection limit in the H₂ gas sensor. To control nanogap size, recent work has demonstrated adjustable nanocrack formation along the *x*- and *y*-axes via the kinetic control of tensile velocities in Pd/polydimethylsiloxane (PDMS) bilayers [17]. A mechanism for the periodic pattern formation was identified: the vertical cracks in the *x*-axis and horizontal cracks in the *y*-axis

Sungyeon Kim and Hyun-Sook Lee are co-first authors.

✉ Sungmee Cho
csmise@yonsei.ac.kr

✉ Wooyoung Lee
wooyoung@yonsei.ac.kr

Sungyeon Kim
neosiren@yonsei.ac.kr

Hyun-Sook Lee
h-slee@hanmail.net

Byungjin Jang
bjjanggun@hanmail.net

¹ Department of Materials Science and Engineering, Yonsei University, 50 Yonsei-ro, Seodaemun-gu, Seoul 03722, Korea

are generated during the stretching and contraction processes, respectively, and are attributed to the differences in the mechanical properties of the metal thin film and the elastomeric substrate. Furthermore, the variation of the tensile velocity ($100\text{--}800\ \mu\text{m s}^{-1}$) changed the density of the nanocrack array under a fixed strain value of 100 %, but the nanogap size was invariant. Although several papers on crack pattern formation have reported that the patterns can be controlled by altering the mechanical strain applied to metal/polymer bilayers at ambient temperature, this approach has not been applied for nanogap-based H_2 sensors [18–22]. Thus, nanogap size control for nanogap-based H_2 sensors still requires study, especially for practical applications in air.

In this work, we quantitatively describe the control of nanocrack pattern formation in a Pd/PDMS bilayer through the application of varying tensile strains (from 30 to 120 %) during mechanical stretching/compression. We correlate the characteristics of the nanocrack patterns in terms of width, density, and strain magnitude. Mechanical nanocrack modulation with variable tensile strains over the entire Pd film is related to the gas detection properties, and this feature allows the film to be used in sensors with low H_2 gas detection limits (50 ppm) in air.

Materials and methods

An elastomeric substrate was fabricated from PDMS according to established literature methods [15]. The PDMS substrate was 1 cm wide \times 2.7 cm long, with a thickness of 0.6–0.75 mm. A 10-nm-thick Pd film with dimensions of 1.0 cm \times 1.5 cm was deposited on the top surface of the PDMS substrate from a high-purity Pd target (3 N) using ultra-high-vacuum (UHV) DC magnetron sputtering under an Ar atmosphere. The deposition process was performed below 2.3×10^{-3} Torr in Ar at a flow rate of 34 sccm and a base pressure of 4.8×10^{-7} Torr. The deposition rate of the Pd film at room temperature (RT) was $\sim 3.7\ \text{\AA s}^{-1}$ at 20 W. The Pd thin films on the PDMS specimens (Pd/PDMS) were loaded onto a microtensile tester (Linkam Scientific Instruments, TST350). Their mechanical properties were measured with a capacity of 5, 7, 11, or 20 N at a constant tensile velocity of $800\ \mu\text{m s}^{-1}$ at tensile strains of 30, 60, 90, and 120 %, respectively. The tensile strain was defined as $\{(L - L_0)/L_0\} \times 100$ (%), where L_0 and L are the initial length of the Pd/PDMS and its length in the presence of a tensile stress, respectively. Nanocracks were intentionally generated on each sample during 25 load/unload cycles at RT. The nanocracks and

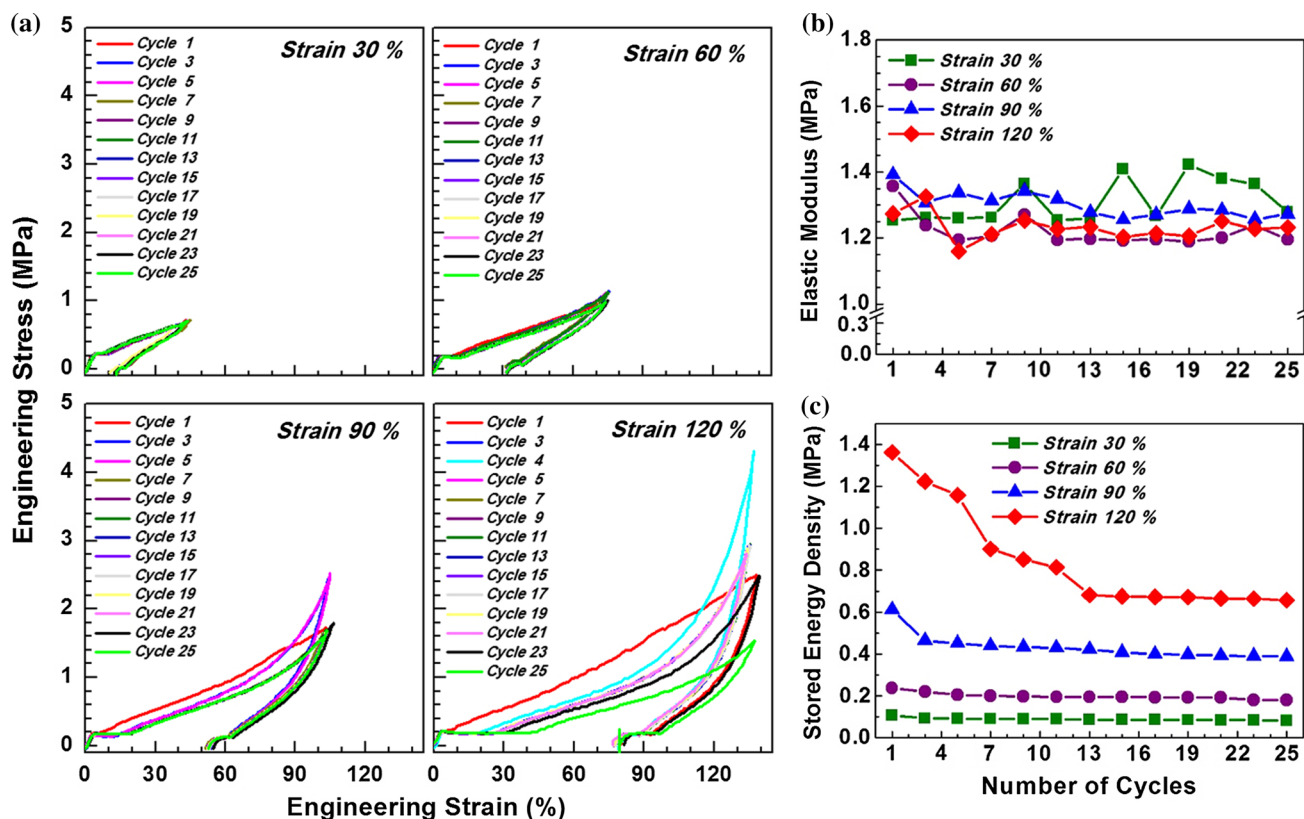


Fig. 1 a Hysteresis loops of tensile stress versus strain for the Pd/PDMS bilayers measured at room temperature with varying strains from 30 to 120 % during 25 load/unload cycles. b Elastic modulus and c stored energy density versus number of cycles for the different tensile strains

surface morphologies of the Pd/PDMS specimens were observed by scanning electron microscopy (SEM, JEOL JSM-6701F), optical microscopy (OM, Olympus BX41 M), and atomic force microscopy (AFM, Park Systems XE-Bio).

For H₂ gas detection measurements, a Pd/PDMS sample was mounted onto a printed circuit board and electrical connections were formed using Ag paste (CANS, ELCOAT P-100). Each sample was exposed to H₂ gas at the rates of 0.005, 0.01, 0.05, 0.1, 0.2, 0.4, 0.8, 1.2, 1.6, and 2 % in air at RT. Sensor measurements were carried out by placing the sensor in a sealed flow cell with a total dead volume of 250 mL and equipped with a mass flow controller. The performance of the H₂ sensor was measured by

monitoring of the change in the resistance in a source-measure unit (Keithley 236, Keithley Instruments Inc.) with a constant voltage supply of 0.1 V for a time interval of 0.1 s. A more detailed procedure can be found elsewhere [10].

Results and discussion

Plots of the tensile stress versus the strain of the Pd/PDMS bilayers obtained at strains of 30–120 % over 25 load/unload cycles are shown in Fig. 1a. The maximum strain value was chosen as 120 % because the samples fractured at strains above 130 %. In all the measurements, the end of

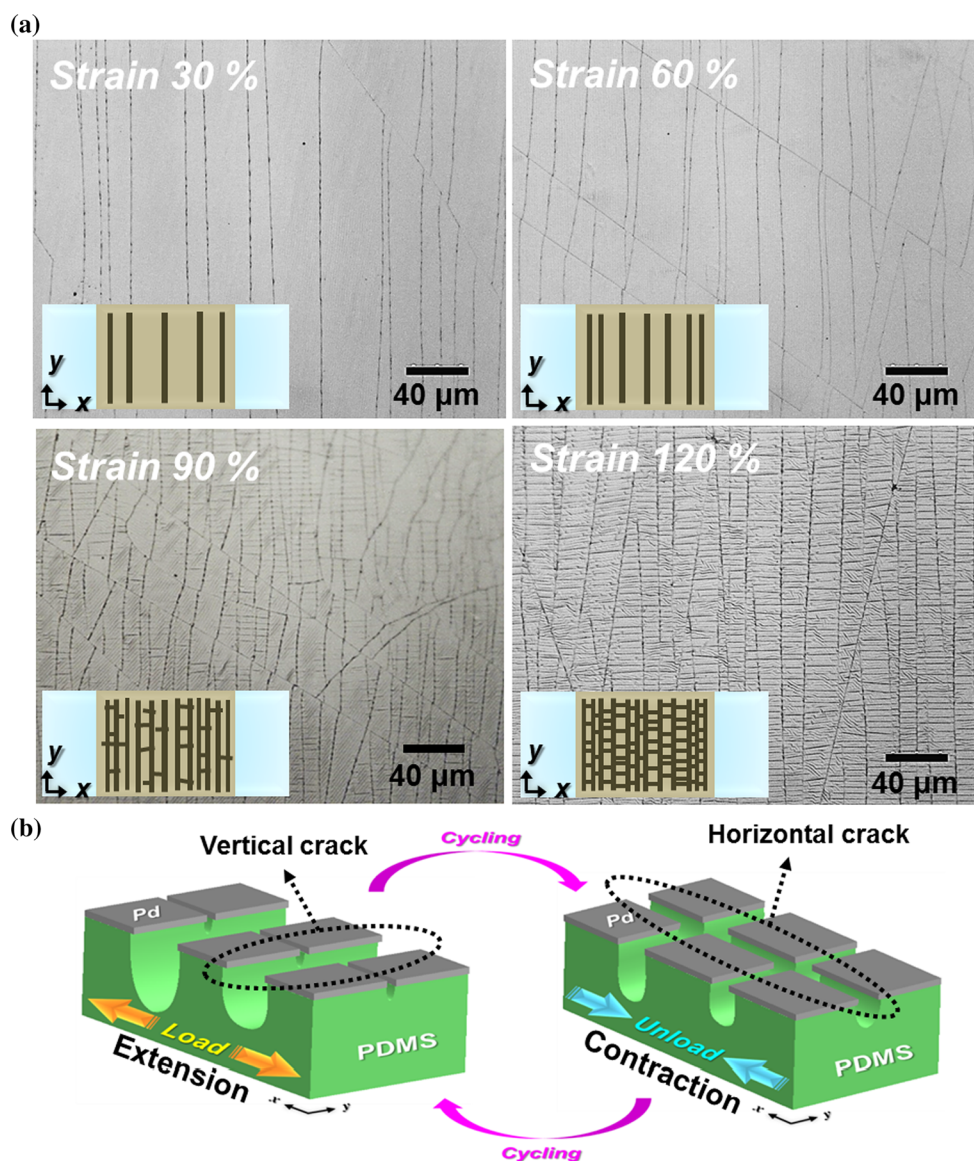


Fig. 2 a Top-view optical microscopy (OM) images of cracks in a Pd thin film on PDMS formed under tensile strains of 30, 60, 90, and 120 %. b Schematic drawing of the mechanism of crack formation during the uniaxial tensile strain cycles

strain was extended to compensate for the changing length of the samples bent at the beginning of the loading state, as can be seen in Fig. 1a. All the loading and unloading stress–strain curves at the different applied strains show hysteresis loops with residual strains. However, the hysteresis loops exhibit external strain- and cycle number-dependent behaviors. At lower tensile strains (30 and 60 %), the loading stress–strain curves are nearly linear and the hysteresis loops are unchanged during cycling. At higher tensile strains (90 and 120 %), the linear curvature at the initial cycle is transformed to non-linear with increasing cycles. The different hysteresis behaviors with respect to strain are mainly attributed to the viscoelasticity of the PDMS. Thus, the thin Pd (10 nm) metal film can be strongly affected by the mechanical behavior of the thick PDMS substrate (0.6–0.75 mm). Viscoelastic materials exhibit both elastic and viscous characteristics when undergoing deformation. The stress–strain curve of such a material is separated into two regimes at a certain strain value depending on the elasticity and viscosity of the material [23], as can be seen in our results in Fig. 1a: a linear viscoelastic regime is observed at lower strains and a time/strain rate-dependent non-linear viscoelastic regime occurs at higher strains. The elastic modulus of the Pd/PDMS, calculated for the strain range below 40 % as the

slope of the initial linear curve [24], shows no change during the entire load/unload cycle (Fig. 1b). This means that the elasticity of the Pd/PDMS at this lower strain is nearly unchanged despite the repeated cycles. However, the viscosity is strongly affected by the magnitude of the external strain and the loading/unloading cycles. Thus, at higher strains of 90 and 120 %, the linear viscoelastic behavior of the hysteresis loops in the initial cycle attains non-linear viscoelastic characteristics with increasing cycles. Moreover, the maximum stress at the end of stretching at the higher strains is suddenly enhanced at around 3–4 cycles and decreases with cycling. These results can be explained as follows: The viscoelastic material exhibits a time delay in returning to its original shape when the load is removed. This property can be exaggerated at higher strains. Therefore, the accumulated energy that remains in the Pd/PDMS material during 1–2 cycles due to its partial recovery causes the sudden enhancement of the maximum viscous stress when the next cycle is applied. Thereafter, the maximum stress is reduced, which is most likely due to strain hardening. On the other hand, Fig. 1c displays the calculated stored strain energy density corresponding to the area of the stress versus strain hysteresis loops from Fig. 1a. At both 90 and 120 % strains, the stored energy density increases during

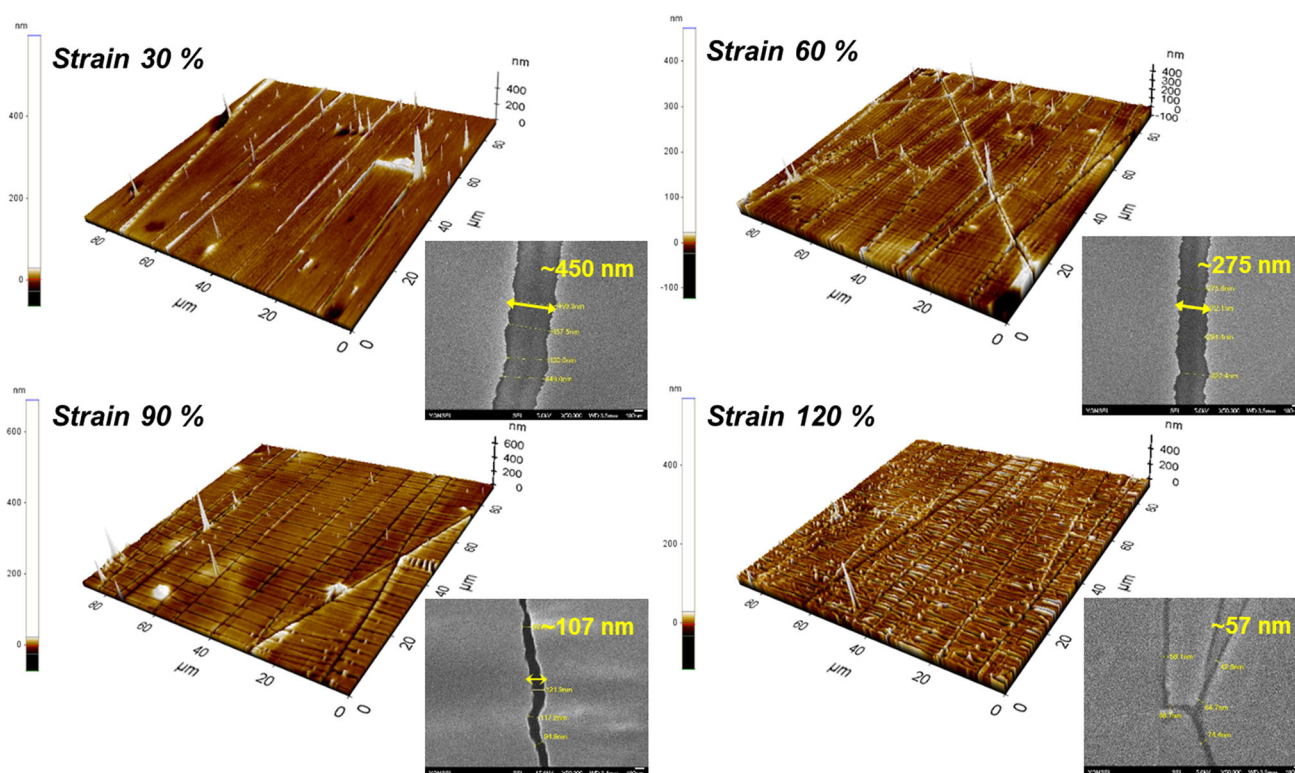


Fig. 3 Atomic force microscopy (AFM) images ($90 \times 90 \mu\text{m}^2$) with cross-section line profiles (x - and y -axes) to observe the various crack patterns formed in Pd/PDMS samples prepared under a tensile strain

gradient. The SEM images in the insets indicate the representative crack width for each tensile strain

the initial cycles and steadily decreases over the multiple repeated loading/unloading cycles. The decrease in the energy density during the cycles implies that the absorbed energy in the samples is used to generate cracks in the Pd film. A significant reduction in the stored energy appears at 120 % strain, which indicates greater crack generation at higher strains. Hence, we microscopically investigated the surfaces of the Pd films strained at different values.

The top-view OM images in Fig. 2a reveal the cracks formed in the Pd thin films on the PDMS substrates. Twenty-five load/unload cycles were applied in the x -direction at tensile strains of 30, 60, 90, and 120 % under a constant tensile velocity of $800 \mu\text{m s}^{-1}$. At low tensile strains (30–60 %), cracks are formed only along the x -direction; however, at 90 % tensile strain, the vertical crack patterning becomes narrower and horizontal crack patterns appear in the y -direction. Finally, many cracks are generated on the Pd film in both the x - and y -directions at the high tensile strain of 120 %. Figure 2b shows a schematic drawing of the mechanism for crack formation under the uniaxial tension strain cycles. As was reported in our previous work, the vertical crack patterns are induced while stretching in the x -direction, and the horizontal crack patterns are created in the y -direction on applying compression to remove the tensile strain, as illustrated in Fig. 2b [17]. The crack formation mechanism was explained by the Poisson effect: the difference in Poisson's ratio ν (i.e., the ratio of the transverse and axial strains, $-\epsilon_{yy}/\epsilon_{xx}$, respectively) between the relatively stiff Pd metal film ($\nu = 0.39$) and the viscoelastic PDMS substrate ($\nu = 0.5$) leads to different stress distributions in those materials [25]. The horizontal cracks observed in the previous study were fabricated under 100 % strain applied at a slow tensile velocity of $50 \mu\text{m s}^{-1}$. In this study, we adopted a higher tensile velocity of $800 \mu\text{m s}^{-1}$ for the strain variations of 30–120 %, and the horizontal cracks appeared only above 90 % [16]. According to these results, we can conclude that the strain required to induce the horizontal cracks must be at least 100 %. Thus, horizontal crack formation is affected by the magnitude of the strain applied to the Pd/PDMS, whereas it is independent of the tensile velocity.

Figure 3 presents more detailed AFM images of the Pd film surfaces on the PDMS substrates. The AFM images show similar crack formation behaviors with strain variation as observed in the OM images in Fig. 2a. In detail, at 30 % tensile strain, we observe a wide distribution of vertical cracks with arrays of partial horizontal buckling; increased buckling arrays are formed along the x - and y -axes as the tensile strain is increased to 60 %. Consequently, these buckled arrays are transformed into nanocracks in both directions at a high tensile strain of 90 %. At 120 %, the distance between adjacent nanocracks becomes narrower in both directions. During crack formation, the

crack widths are also narrowed, as can be seen in the representative SEM images in the insets of Fig. 3.

Average nanocrack widths for the various tensile strains were estimated from SEM images obtained at 9 points in the Pd thin films ($1.0 \times 1.5 \text{ cm}^2$), as shown in Fig. 4a. The vertical and horizontal cracks, formed along the x - and y -directions, respectively, show different width variations for the different tensile strains. The average widths of the vertical nanocracks are 357, 254, 104, and 94 nm at 30, 60, 90, and 120 % tensile strains, respectively, and those of the horizontal nanocracks are 52 and 41 nm at 90 and 120 % tensile strains, respectively. The average width of the vertical cracks formed at 30 % strain is consistent with prior published works for an as-cracked Pd/PDMS strained at 25 % with 300–420 nm gap size [10, 13]. In contrast to the previous result showing the independence of crack formation on the tensile velocity at a fixed strain, the vertical crack width in this study shows a significant decrease with increasing tensile strain from 30 to 90 % [17]. However, the horizontal crack widths at 90 and 120 % strains look similar. The average crack density in a unit length along the two axes was calculated by counting the peaks in the AFM depth profiles scanned at 9 positions

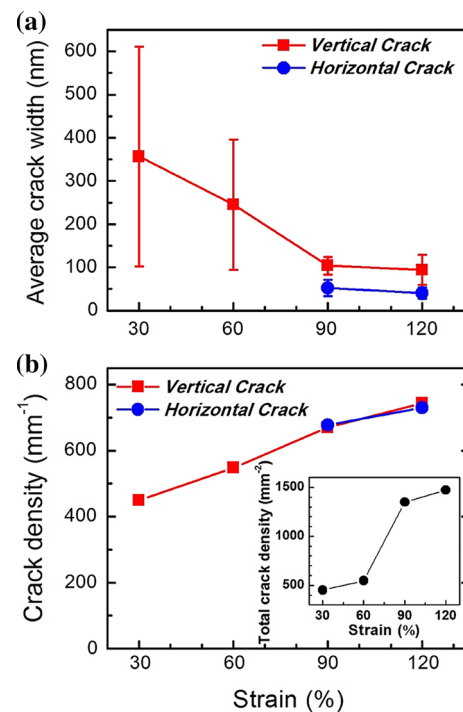


Fig. 4 **a** Average crack width distribution along the x - and y -axes estimated from SEM images in Fig. 3. **b** Crack density in a unit length for both the x - and y -axes, which was calculated from the AFM depth profiles at various tensile strains. Inset shows the average total crack density per unit area. In both **a** and **b**, data points for the horizontal cracks at strains of 30 and 60 % are absent because the horizontal cracks appear only above strains of 90 %

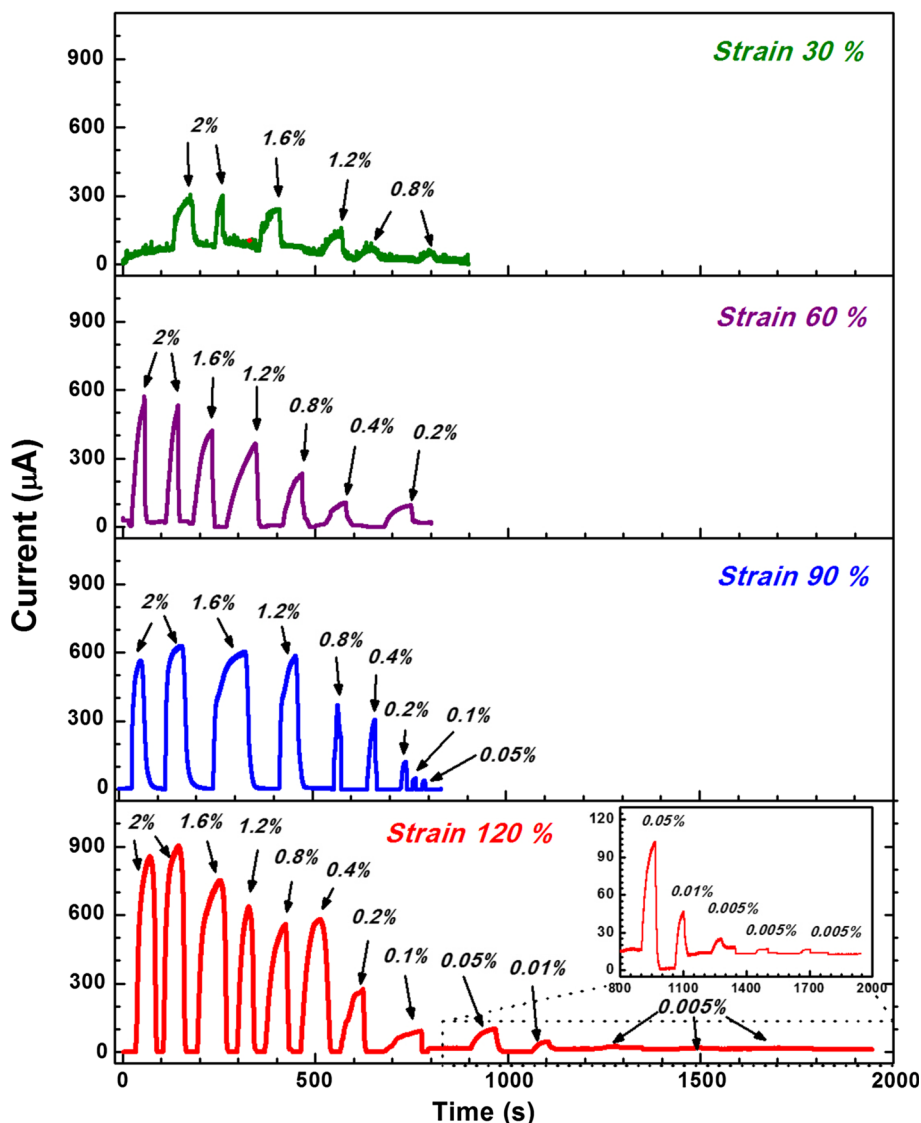


Fig. 5 Real-time current responses of the Pd/PDMS prepared under the indicated strains, which were evaluated during exposure to H₂ gas concentrations ranging from 0.005 to 2 % in air

($90 \times 90 \mu\text{m}^2$) across the entire film area ($1.0 \times 1.5 \text{ cm}^2$). The vertical crack density gradually increases as the tensile strain increases, and the horizontal crack density (above 90 % strain) is also increased. Therefore, the total crack density per unit area shows a sudden increase on going from 60 to 90 % applied strain.

To examine the effects of the tensile strain, the real-time electrical responses upon gradually decreasing the H₂ concentration from 2 to 0.005 % were measured in air for the variously cracked Pd/PDMS samples. The results are shown in Fig. 5. The cracked Pd films on PDMS operated in a satisfactory ON–OFF mode over the measured H₂ concentration range. As the tensile strain was increased from 30 to 120 %, the limits of H₂ gas detection were decreased to 0.8, 0.2, 0.05, and 0.005 %, respectively, as

can be seen in Fig. 6a. To evaluate the H₂ sensing performance of the nanocracked Pd/PDMS, the response time (defined as the time to reach 90 % from 10 % of the maximum electrical resistance) and recovery time (defined as the time to reach 10 % from 90 % of the baseline resistance) were estimated. At 2 % H₂, the average response and recovery times are in the range of 12–36 and 5.5–40 s, respectively, which are faster by approximately an order of magnitude that those reported for a Pd nanowire ($88 \times 128 \text{ nm}^2$) measured at 2 % H₂ in air [26]. In addition, the average response time in 2 % H₂ becomes shorter with increasing strain, which may be caused by the higher crack density with narrower widths.

Here, a noteworthy fact is that the sensor subjected to a high strain of 120 % reveals a very low detection limit of

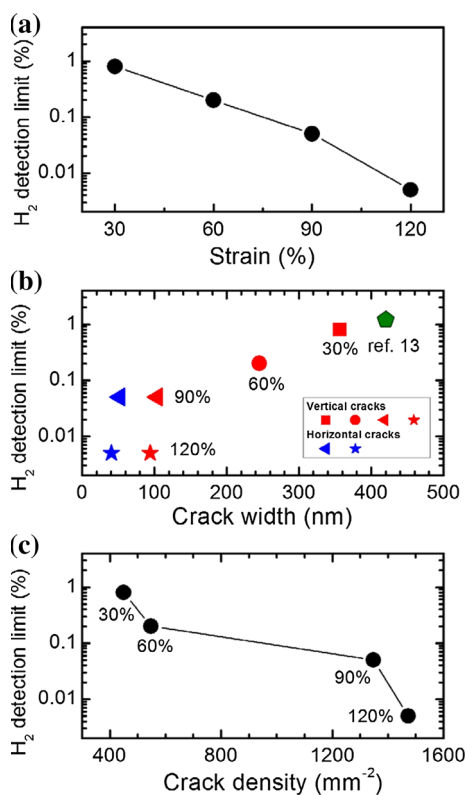


Fig. 6 Limit of hydrogen detection as a function of **a** strain, **b** crack width, and **c** crack density for the pure Pd-based PDMS H₂ sensors (Color figure online)

0.005 % even in air, as clearly seen in the magnified view in Fig. 5. This remarkable reduction in the H₂ gas detection limit in air is comparable to the values for Pd-based sensors with very narrow nanogaps (25–100 nm) measured under nitrogen background gas [10, 12, 13]. When the Pd/PDMS sensor is exposed to H₂ in air, O₂ molecules react with the surface of the Pd film to form chemisorbed O atoms; then, the reaction of the Pd surface with chemisorbed H₂ results in both Pd–H and H₂O formation according to the following reactions: Pd–O + 3/2H₂ (ads) → Pd–H + H₂O (ads) and H₂O (ads) → H₂O (g) [27]. Accordingly, the rate of Pd–H formation in air is reduced compared to that under a N₂ atmosphere. Thus, it is usually difficult to achieve such a low limit for H₂ gas detection in air (0.005 %) for a Pd-based nanogap sensor. The pure Pd/PDMS sensor with a nanogap size of ~420 nm exhibited a H₂ gas detection limit of 1.2 %, as presented earlier (green pentagon in Fig. 6b). In order to explain our results, we considered the width and density of the nanocracks as important factors. The previous studies in N₂ environments revealed that the reduction in the crack width is a significant factor for the detection of low H₂ concentrations [10–16]. Our results consistently demonstrate the same behavior, i.e., the decrease of the gas detection limit with decreasing

nanocrack width, from 30 to 90 % strain. However, although the crack widths of the Pd/PDMS specimens strained at 90 and 120 % are similar, the detection limits are much lower for the 120 % sample. Hence, the higher crack density at 120 % than at 90 % as observed in Fig. 6c must inevitably be the reason. Moreover, it has been predicted that the surface area/volume ratio would proportionally give a high performance in H₂ gas detection properties for low H₂ levels (<1 %) [26]. Hence, the Pd/PDMS produced by 120 % strains provides a much larger surface area in the densely propagated periodic nanocrack patterns in both the *x*- and *y*-directions, and the reaction to form Pd–H can easily occur at the Pd cracked surfaces, even at the lowest H₂ concentration, compared to the case of 90 % strain. Therefore, the excellent H₂ gas detection properties—i.e., the lowest detection limit of 0.005 % in air at the high strain of 120 %—are primarily attributed to the formation of many narrow nanocracks created over the entire Pd film, allowing rapid connection between neighboring nanocracks by the volume expansion of the Pd film after H₂ gas exposure.

Conclusions

The strategy of applying various tensile strains shows great promise for generating quantitatively ordered crack patterns in Pd thin films on PDMS, as well as their application in H₂ sensors with low detection limits in air. In the hysteresis loops of tensile stress versus strain, the decrease in the stored energy during the loading/unloading cycles implies internal crack propagation and leads to further crack generation at higher tensile strains. We found that the horizontal cracks parallel to the straining direction can be generated only when the tensile strain is above 90 % and are independent of the tensile velocity, and provide quantitatively ordered crack patterns over the entire Pd film surface. At the high tensile strain of 120 %, the high density of vertical and horizontal cracks with narrow gaps and resultant high surface area in the Pd/PDMS specimens gives rise to the very low detection limit of 50 ppm H₂, even in air. Thus, we have demonstrated that the density of nanocracks is critical for detecting low H₂ concentrations. These results provide a simple mechanism for controlling the detection properties of H₂ gas sensors with low detection limits, even in air.

Acknowledgements This work was supported by the Priority Research Centers Program through the National Research Foundation of Korea (NRF) funded by the Ministry of Education, Science and Technology (2009-0093823). This subject is also supported by Korea Ministry of Environment as Convergence Technology Program (2015001650001).

References

1. Varghese OK, Gong D, Paulose M, Ong KG, Grimes CA (2003) Hydrogen sensing using titania nanotubes. *Sens Actuator B* 93:338–344
2. Rout CS, Krishna SH, Vivekchand SRC, Govindaraj A, Rao CNR (2006) Hydrogen and ethanol sensors based on ZnO nanorods, nanowires and nanotubes. *Chem Phys Lett* 418:586–590
3. Wang B, Zhu LF, Yang YH, Xu NS, Yang GW (2008) Fabrication of a SnO₂ nanowire gas sensor and sensor performance for hydrogen. *J Phys Chem C* 112:6643–6647
4. Lu C, Chen Z (2009) High-temperature resistive hydrogen sensor based on thin nanoporous rutile TiO₂ film on anodic aluminum oxide. *Sens Actuator B* 140:109–115
5. Zhu LF, She JC, Luo JY, Deng SZ, Chen J, Xu NS (2010) Study of physical and chemical processes of H₂ sensing of Pt-coated WO₃ nanowire films. *J Phys Chem C* 114:15504–15509
6. Sun B, Horvat J, Kim HS, Kim W-S, Ahn J, Wang G (2010) Synthesis of mesoporous α -Fe₂O₃ nanostructures for highly sensitive gas sensors and high capacity anode materials in lithium ion batteries. *J Phys Chem C* 114:18753–18761
7. Zhao M, Wong MH, Huang JX, Ong CW (2014) Ultrathin percolated WO₃ cluster film and its resistive response to H₂. *J Alloys Compd* 612:163–169
8. Hoa ND, Quy NV, Jung H, Kim D, Kim H, Hong S-K (2010) Synthesis of porous CuO nanowires and its application to hydrogen detection. *Sens Actuator B* 146:266–272
9. Ueda Y, Tokuda Y, Yoko T, Takeuchi K, Kolesnikov AI, Koyanaka H (2012) Electrochemical property of proton-conductive manganese dioxide for sensing hydrogen gas concentration. *Solid State Ionics* 225:282–285
10. Lee J, Shim W, Lee E, Noh J-S, Lee W (2011) Highly mobile palladium thin films on an elastomeric substrate: nanogap-based hydrogen gas sensors. *Angew Chem Int Ed* 50:5301–5305
11. Lee EY, Lee J, Noh J-S, Kim W, Lee T, Maeng S, Lee W (2012) Pd–Ni hydrogen sponge for highly sensitive nanogap-based hydrogen sensors. *Int J Hydrog Energy* 37:14702–14706
12. Chang T, Jung H, Jang B, Lee J, Noh J-S, Lee W (2013) Nanogaps controlled by liquid nitrogen freezing and the effects on hydrogen gas sensor performance. *Sens Actuator A-Phys* 192:140–144
13. Jang B, Lee K-Y, Noh J-S, Lee W (2014) Nanogap-based electrical hydrogen sensors fabricated from Pd-PMMA hybrid thin films. *Sens Actuator B* 193:530–535
14. Lee YT, Jung H, Nam SH, Jeon PJ, Kim JS, Jang B, Lee W, Im S (2013) Sensing extremely limited H₂ contents by Pd nanogap connected to an amorphous InGaZnO thin-film transistor. *Nanoscale* 5:8915–8920
15. Lee J, Noh J-S, Lee S-H, Song B, Jung H, Kim W, Lee W (2012) Cracked palladium films on an elastomeric substrate for use as hydrogen sensors. *Int J Hydrog Energy* 37:7934–7939
16. Jung H, Jang B, Kim W, Noh J-S, Lee W (2013) Ultra-sensitive, one-time use hydrogen sensors based on sub-10 nm nanogaps on an elastomeric substrate. *Sens Actuator B* 178:689–693
17. Kim S, Jang B, Park J, Lee Y-K, Lee H-S, Cho S, Lee W (2015) *Sens Actuator B*, under review
18. Schmoller KM, Bausch AR (2013) Similar nonlinear mechanical responses in hard and soft materials. *Nat Mater* 12:278–281
19. Chung JY, Lee J-H, Beers KL, Stafford CM (2011) Stiffness, strength, and ductility of nanoscale thin films and membranes: a combined wrinkling–cracking methodology. *Nano Lett* 11:3361–3365
20. Im SH, Huang R (2005) Evolution of wrinkles in elastic-viscoelastic bilayer thin films. *J Appl Mech-Trans ASME* 72:955–961
21. Xu B, Chen D, Hayward RC (2014) Mechanically gated electrical switches by creasing of patterned metal/elastomer bilayer films. *Adv Mater* 26:4381–4385
22. Kim BC, Matsuoka T, Moraes C, Huang J, Thouless MD, Takayama S (2013) Guided fracture of films on soft substrates to create micro/nano-feature arrays with controlled periodicity. *Sci Rep* 3:3027
23. Ewoldt RH, Hosoi AE, McKinley GH (2009) Nonlinear viscoelastic biomaterials: meaningful characterization and engineering inspiration. *Integr Comp Biol* 49:40–50
24. Mills KL, Zhu X, Takayama S, Thouless MD (2008) The mechanical properties of a surface-modified layer on polydimethylsiloxane. *J Mater Res* 23:37–48
25. Lakes R (1993) Advances in negative Poisson's ratio materials. *Adv Mater* 5:293–296
26. Yang F, Kung S-C, Cheng M, Hemminger JC, Penner RM (2010) Smaller is faster and more sensitive: the effect of wire size on the detection of hydrogen by single palladium nanowires. *ACS Nano* 4:5233–5244
27. Yang F, Donovan KC, Kung S-C, Penner RM (2012) The surface scattering-based detection of hydrogen in air using a platinum nanowire. *Nano Lett* 12:2924–2930